

Carbon nanotube field emitters

Alexander Zhibanov^{1,2}, Evgeny Pogorelov¹ and Yia-Chung Chang¹

¹*Research Center for Applied Sciences, Academia Sinica, Taiwan*

²*Department of Mechatronics, Gwangju Institute of Science and Technology, Korea*

1. Introduction

Application of various one-dimensional nanostructure materials as field emission sources has attracted extensive scientific efforts. Elongated structures are suitable for achieving high field-emission-current density at a low electric field because of their high aspect ratio. Area of its application includes a wide range of field-emission-based devices such as flat-panel displays, electron microscopes, vacuum microwave amplifiers, X-ray tube sources, cathode-ray lamps, nanolithography systems, gas detectors, mass spectrometers etc.

Since the discovery of carbon nanotubes (CNTs) (Iijima, 1991; Iijima & Ichihashi, 1993; Bethune et al., 1993) and experimental observations of their remarkable field emission characteristics (Rinzler et al., 1995; de Heer et al., 1995; Chernozatonskii et al., 1995), significant efforts have been devoted to the application of using CNTs for electron sources.

One of the main problems for design such field emission emitter is the difficulties in estimation of the electric field on the apex of nanotubes. Only a few works considered forces acting on nanoemitters under electric field. Thus far, there is no analytical formula which provides a good approximation to the total current generated by the nanoscale field emitter. In this chapter, we theoretically consider the electric field strength, field enhancement factor, ponderomotive forces, and total current of a metallic elliptical needle in the form of hemi-ellipsoid in the presence of a flat anode. Also we shortly review the history CNT cold emitters and technology of their fabrication. Furthermore we consider the application areas of CNT electron sources.

2. Historical preview

Field emission is an emission of electrons from a solid surface under action of external high electric field E . Field emission was experimentally discovered in 1897 by R.W. Wood (Wood, 1897). In 1929 R.A. Millikan and C.C. Lauritsen established linear dependence of the logarithm of current density on $1/E$ (Millikan & Lauritsen, 1929). Field emission was explained by quantum tunneling of electrons through the surface potential barrier. This theory was developed by R.H. Fowler and L.W. Nordheim in 1928 (Fowler & Nordheim, 1928).

According to the Fowler-Nordheim theory, the current density of the field emission j is determined by the following expression

$$j \approx \frac{C_1 E^2}{\phi} \exp\left(-\frac{C_2 \phi^{3/2}}{E}\right), \quad (1)$$

where j denotes the emission current density in Acm^{-2} , E is local electric field at the emitting surface in Vcm^{-1} , ϕ is work function in eV, and the first and second Fowler-Nordheim constants are $C_1 = 1.56 \times 10^{-6} \text{ AeVV}^{-2}$, $C_2 = 6.83 \times 10^7 \text{ VeV}^{-3/2}\text{cm}^{-1}$, respectively. The electric field E at the CNT tip increases compared with the average field E_0 . Substituting in Eq. (1) the expression $E = \beta E_0$, where β is a field enhancement factor, we shall write the Fowler-Nordheim dependence in the form:

$$j \approx \frac{C_1 (\beta E_0)^2}{\phi} \exp\left(-\frac{C_2 \phi^{3/2}}{\beta E_0}\right). \quad (2)$$

Thus current-voltage characteristics of the field electron emission in the Fowler-Nordheim coordinates $(\log j/E_0^2, 1/E_0)$ are presented by straight lines. It was assumed that $\phi = 4.8 \text{ eV}$ for nanotubes. The field enhancement factor β varied from 300 to 3000 depending on the tube size.

Theory of field emission considered in details in recent books (Furse, 2005; Ducastelle et al., 2006).

Strong electric fields ($E \sim 10^7 \text{ Vcm}^{-1}$) near a surface are necessary to obtain the appreciable field emission current from pure metals. Therefore, the emitters in early investigations were produced in the form of thin spike with radiuses of curvature on the ends about 1 micron.

Development of lithographic techniques allowed fabricating so called "Spindt tips" in which the field emitters are small sharp molybdenum microcones. One of the first papers describing such technology has appeared in 1968 (Spindt, 1968). Essential efforts have been spent by several companies for development of the Spindt-type field emission display, but no large-screen production has been forthcoming.

The new potential in designing field emitters and devices on their basis has appeared after discovery of carbon nanotubes.

Field emission of carbon nanotubes was for the first time reported by Fishbine (Phillips Lab.) (Fishbine et al., 1994), Gulyaev (Institute of Radio-engineering and Electronics, Russia) (Gulyaev et al., 1994), and Rinzler (Rice University) (Rinzler et al., 1994) in 1994.

Four first journal papers (Gulyaev et al., 1995; Chernozatonskii et al., 1995; Rinzler et al., 1995; de Heer et al., 1995) dedicated to this problem were published in 1995. As is known, several papers have appeared in the two subsequent years: two works (Chernozatonskii et al., 1996; Collins & Zettl, 1996) were published in 1996 and seven works (Collins & Zettl, 1997; Gulyaev et al., 1997; Sinitsyn et al., 1997; de Heer et al., 1997; Saito et al., 1997a; Saito et al., 1997b; Lee et al., 1997) were published in 1997. Starting from 1998, interest in field-emission properties of CNT was increasing explosively all over the world. Today we can speak of thousands of published papers.

Recently, field emission from metals (Lee et al., 2002), metal oxides (Li et al., 2006; Banerjee et al., 2004; Jo et al., 2003; Seelaboyina et al., 2006), metal carbides (Charbonnier et al., 2001), and other elongated nanostructures have also been explored. It is now possible to control the diameter, height, radius of curvature of the tip, and basic form of emitters during growth. Elongated structures of different shapes such as nanotubes, nanocones, nanofibers,

nanowires, nanoneedles, and nanorods have been successfully grown (Li et al., 2006; Li et al., 2007; Jang et al., 2005; Hu & Huang, 2003).

Promising new materials for field-emission sources are B- and N-doped CNTs. Terrones et al. (Terrones et al., 2004; Terrones et al., 2008) have reviewed the field emission properties of B- and N-doped CNTs and nanofibres. B-doped multi-wall CNTs could exhibit enhanced field emission (turn on voltages of ~ 1.4 V/ μm) when compared to pristine multi-wall CNTs (turn on voltages of ~ 3 V/ μm). N-doped CNTs are able to emit electrons at relatively low turn-on voltages (2 V/ μm). This phenomenon arises from the presence of B atoms (holes) or N atoms (donors) at the nanotube tips.

3. Carbon nanotubes field emitters

3.1 Physical properties of carbon nanotubes suitable for cold emission

From the practical application point of view CNTs are preferable field emitters due to their low threshold voltage, good emission stability and long emitter lifetime.

CNTs possess these advantages due to the large aspect ratio, high electric and thermal conductivity, highest flexibility, elasticity, and Young's modulus. Their strong covalent bonding makes them chemically inert to poisoning and physically inert to sputtering during field emission. They can also carry a very high current density of order 10^9 A cm^{-2} before electromigration. Nanotubes have a high melting point and preserve their high aspect ratio over time. CNTs emits electrons under conditions of technical vacuum. They are chemically inert to poisoning due to strong covalent bonding. Measuring of field emission properties (Kung et al., 2002) and theoretical ab-initio calculations (Park et al., 2001) shows that emission currents are significantly enhanced when oxygen is adsorbed at the tip of carbon nanotubes.

3.2 Manufacturing techniques for CNT-based field-emission cathodes

Many technologies for fabrication of CNT-based field-emission cathodes were offered. We shall consider only some of them.

Individual CNT field emitters have a large potential for application in electron guns for scanning electron microscopes. To investigate the emission properties of individual CNTs de Jonge et al (de Jonge & Bonard, 2004) improved the mounting method using a piezo-driven nanomanipulator. For the mounting of an individual CNT on a tungsten tip, a tungsten wire was fixed by laser-welding on a titanium (or tungsten) filament.

Field emission CNT-based cathodes are manufactured either as a bulk solid containing nanotubes or as a film with thickness from hundreds of nanometers to tens of microns.

Bulk cathodes are known to be manufactured by two methods. The Alex Zettl team from California University, Berkley, USA used a technology in accordance with which the ready material of unsorted randomly aligned nanotubes is mixed into a compound, baked, and surface ground. Flexible and elastic nanotubes are not broken during the grinding. In accordance with the technology used by the Yahachi Saito team of Mie University (Japan), the graphite-electrode material processed by an electric arc is cut to pellets and glued to a stainless-steel plate by silver paste.

Film technologies are used in all other cases. Film cathodes are basically manufactured by two methods: either preliminary synthesized tubes are attached to a substrate or the tubes are grown directly on the substrate.

In the two methods, different technologies yield films of both well oriented and strongly entangled tubes.

N.I. Sinitsyn group from Institute of Radio-engineering and Electronics (Saratov, Russia) used CVD methods for synthesizing films of both regularly grown nanotubes (Fig. 1) and “felt” of entangled fibers. Strips were obtained using a catalyst deposited through a template (Zhbanov et al., 2004).

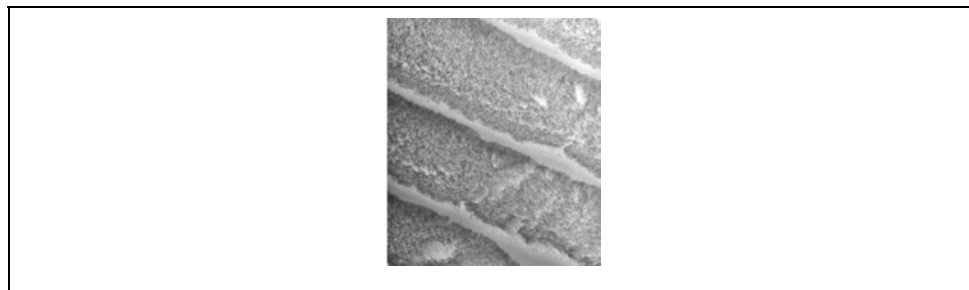


Fig. 1. Photograph of strips of oriented CNTs synthesized on a substrate. The strip width is $20\ \mu\text{m}$ and the gap between the strips is $5\ \mu\text{m}$ (Zhbanov et al., 2004).

The Jean-Marc Bonard team of Lousanne Polytechnical School (Switzerland) developed the technology of microcontact printing of catalytic precursor for growing oriented tubes arranged in accordance with a specified pattern on a substrate (Bonard et al., 2001b). The catalyst, the so-called “ink”, was applied to the stamp surface. The ink was a solution containing from 1 to 50 mM of $\text{Fe}(\text{NO}_3)_3 \cdot 9\text{H}_2\text{O}$. The duration of contact during the printing was 3 s. Nanotube deposition was by the CVD method in a standard flow reactor at a temperature of $720\ ^\circ\text{C}$.

In the case of low concentration of catalyst (1 mM, Fig. 2a), several single nanotubes are randomly distributed over the printing region. The catalyst-concentration growth is accompanied by formation of films of entangled tubes, as is shown in Figs. 2b and 2c. For concentrations about 50 mM, clusters of nanotubes oriented normally to the surface are formed. Figure 2d shows that the sides of the walls are flat, and not a single tube is hanging outward. For concentrations above 60 mM, growth of nanotubes is retarded, and the printed template is covered by amorphous carbon particles.

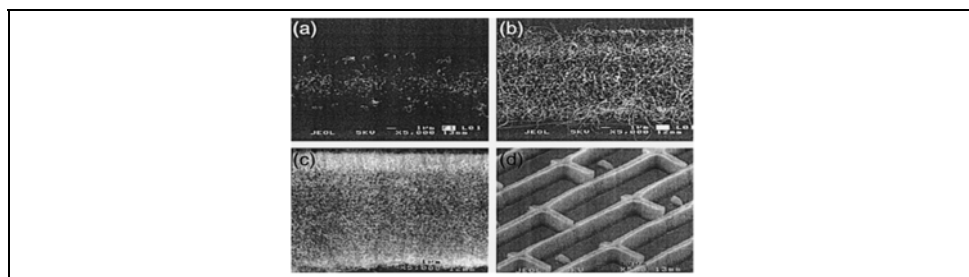


Fig. 2. Nanotube growth for various concentrations of catalytic ink used for the precursor application. Catalyst concentration in the solution was 1 mM (a), 5 mM (b), 40 mM (c), and 50 mM (d). The figure is taken from (Bonard et al., 2001b).

Hongjie Dai team of Stanford University, USA, used the following technology for obtaining arrays of well-oriented carbon nanotubes. First, porous silicon was formed on the surface of a silicon substrate by anode etching and then the ferrum film was deposited on the latter through the shadow mask by electron-beam evaporation (Fan et al., 1999). Then nanotubes were grown as a result of acetylene decomposition in argon flow at 700 °C.

E. F.Kukovitsky team of the Kazan Physics-Technical Institute (Russia) developed the technology of synthesis of oriented nanotubes with conical layers (Fig. 3) (Musatov et al., 2001; Kukovitsky et al., 2003). The first stage of the process involves polyethylene pyrolysis in the first oven at a temperature of 600 °C. Then, by the helium flow, the gaseous products of pyrolysis are transferred to the second oven where nanotubes grow on the nickel foil catalyst at a temperature of 800 to 900 °C. For the obtained specimens, the current density was 10 mA/cm² for the electric field from 4 to 4.5 V/μm.

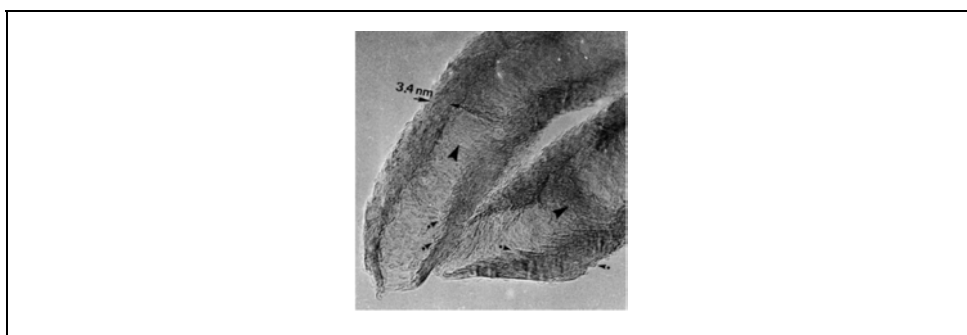


Fig. 3. High-resolution electron microscope image of nanotubes with conical layers. Graphene layers are marked by arrows with points, and the CNT growth direction is marked by large arrows (Musatov et al., 2001).

As is obvious from the literature analysis, almost all CNT-based cathodes show high emission irrespective of the fact whether the tubes are multi-wall or single-wall, well-oriented or entangled. Bamboo-shaped aligned carbon nanotubes (Srivastava et al., 2006; Ghosh et al., 2008) as well as carbon nanocones (Yudasaka et al., 2008) demonstrate high field electron emission.

Let's note, that not only elongated carbon nanotubes, but also pyramids from fullerenes are used as cold cathodes. Formation and characteristics of fullerene coatings on the surface of tungsten tip field emitters and emitters with ribbed crystals formed on their surface are studied by group of Sominskii from St. Petersburg State Technical University (Russia) (Tumareva et al., 2002; Tumareva et al., 2008). Methods of creating microprotrusions on the surface of the coatings that considerably enhance the electric field have been developed and tested. Emitters with a single microprotrusion demonstrated emission current densities up to 10⁶-10⁷ A/cm². It was shown that single micron-sized emitters can stably operate at currents up to 100 μA.

3.3 Electric field and field enhancement factor in diode configuration

The field enhancement factor is very important parameter for characterization of CNT emitters.

The model of a hemisphere on a post for CNT emitters is widely used in analytical approximations and numerical simulations (Fig. 4). To calculate the electric-field intensity and the field enhancement factor on the nanotube tips, the following assumptions are usually done:

- 1) Nanotubes are regularly located on a flat substrate in a “honeycomb-like” order. A nanotube is a cylinder with height h and diameter 2ρ capped by a hemisphere of ρ radius. Total height of closed nanotube is H , the distance from cathode to anode is L , the gap between anode and nanotube tip is l , and the distance between the nearest neighbors is D .
- 2) A nanotube obeys the laws of continuous medium, is perfectly conducting, and the cathode potential is maintained on its entire surface.

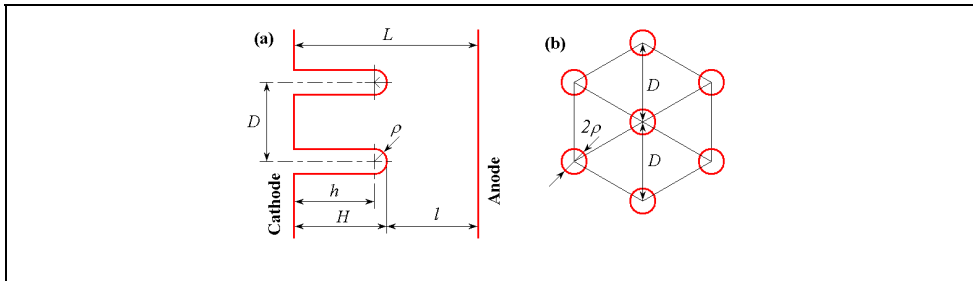


Fig. 4. Scheme of aligned nanotube film, the model of a hemisphere on a post: (a) side view; (b) top view.

Let us introduce dimensionless parameters for the geometrical characterization of model. The dimensionless height of emitter, the dimensionless gap between anode and emitter tip, and the dimensionless distance between individual emitter are the following:

$$\eta = \frac{\rho}{h}, \quad \lambda = \frac{\rho}{l}, \quad \delta = \frac{\rho}{D}. \tag{3}$$

Until now the analytical solution for the model of a hemisphere on a post is unknown. There is no even a solution for the individual cylindrical nanotube closed by hemispherical cap in a uniform electric field.

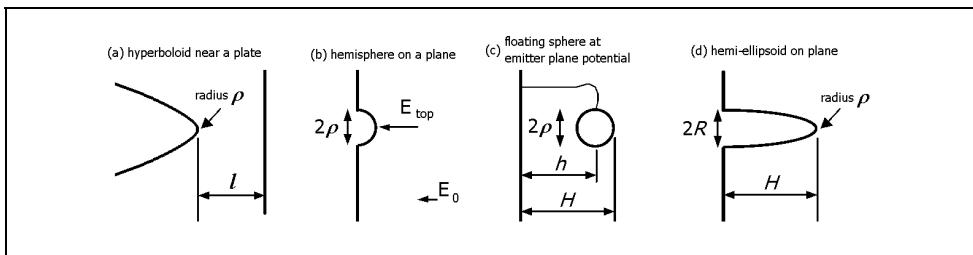


Fig. 5. Schemes of simplest models for field enhancement factor estimation: (a) hyperboloid near a plate; (b) hemisphere on a plane; (c) floating sphere at emitter-plane potential, and (d) hemi-ellipsoid on a plane.

Numerical simulations were reported in many papers (Edgcombe & Valdrè, 2001; Edgcombe & Valdrè, 2002; Read & Bowring, 2004; Musatov et al., 2001). Calculation difficulties in these numerical methods arise due to the large nanotube aspect ratio and very long distance between cathode and anode in comparison with emitter height. Usually, these numerical results were generalized and simple fitting formulas of field enhancement factor for individual nanotube (Edgcombe & Valdrè, 2001; Edgcombe & Valdrè, 2002; Read & Bowring, 2004; Shang et al., 2007), for nanotube in space between parallel cathode and anode planes (Bonard et al., 2002a; Filip et al., 2001; Nilsson et al., 2002; Smith et al., 2005), and for a nanotube surrounded by neighboring nanotubes with a screening effect (Jo et al., 2003; Glukhova et al., 2003; Nilsson et al., 2000; Read & Bowring, 2004; Wang et al., 2005) were suggested. The main problem for such algebraic fitting formulas is the lack of a definitive proof of their accuracy.

Four of the simplest models are the “hyperboloid near a plate” model, the “hemisphere on a plane” model, the “floating sphere at emitter-plane potential” model, and the “hemellipsoid on plane” model. We follow to the classification suggested by Forbes *et al.* (Forbes et al., 2003).

These models allows analytical solutions, they are illustrated in Fig.5. We will use dimensionless parameters Eq. (3) to define geometry of these models.

3.3.1 Hyperboloid near a plate model

We introduce the prolate spheroidal coordinates σ and τ to consider the model of a hyperboloid near a plate (Fig. 6).

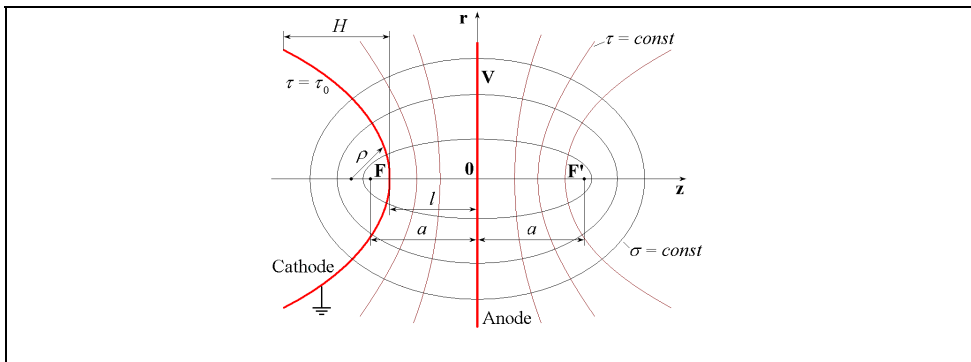


Fig. 6. Hyperboloid near a plate in prolate spheroidal coordinates.

The equation of prolate spheroid is:

$$\frac{r^2}{a^2(\sigma^2 - 1)} + \frac{z^2}{a^2\sigma^2} = 1; \sigma \geq 1. \quad (4)$$

The equation of hyperboloid of two sheets is:

$$\frac{r^2}{a^2(\tau^2 - 1)} + \frac{z^2}{a^2\tau^2} = 1; \quad 1 \geq \tau \geq -1. \quad (5)$$

Points $F(0; -a)$ and $F'(0; a)$ are the foci of the hyperboloids and spheroids. The cathode represents a hyperboloid of revolution $\tau_0 = const$ and the anode is a plane $\tau = 0$. They are shown in Fig. 6 by solid red lines. The radius of hyperboloid curvature of the tip is ρ . The electric field is calculated according to the formula:

$$E = \frac{V}{a\sqrt{(\sigma^2 - \tau^2)(1 - \tau^2)} \operatorname{arctanh}(l/a)}, \quad (6)$$

where function $\operatorname{arctanh}$ is inverse hyperbolic tangent, V is the voltage applied across a gap between anode and cathode.

The model of a hyperboloid near a plate is suitable to describe the interaction of individual CNT field emitter with surface in scanning electron microscopes. Usually in cases important for practice we have $\rho \ll l$ and $l \ll H$.

If $\rho \ll l$ the maximal value of the module of intensity is approximated by the formula (Drechsler & Müller, 1953):

$$E_{top} \approx \frac{V}{\rho \ln(4l/\rho)}. \quad (7)$$

If we define the macroscopic field by $E_0 = V/l$ then we can write the field enhancement factor

$$\beta = \frac{\sqrt{1 + \lambda}}{\lambda \cdot \operatorname{arctanh}\sqrt{1/(1 + \lambda)}}. \quad (8)$$

Let us estimate the electric force acting on the surface of ellipsoid. The electrostatic force acting on the elementary area, s of the external surface is given by

$$\vec{F} = \int_s \frac{\epsilon_0}{2} E^2 \vec{n} ds, \quad (9)$$

where ϵ_0 is the electric constant, \vec{n} is a vector normal to the surface.

Taking into account that the infinitesimal surface element is $ds = 2\pi a^2 \sqrt{(1 - \tau_0^2)(\sigma^2 - \tau_0^2)} d\sigma$, we can analytically integrate the force acting on the top of a hyperboloid surface of height H (see Fig. 6). It is clear that r -component of force equals to zero, $F_r = 0$. For the z -component we have

$$F_z(H) = \frac{\pi\epsilon_0 V^2}{2 \operatorname{arctanh}^2 \sqrt{1/(1 + \lambda)}} \ln \left(1 + \frac{2H}{\rho} + \frac{2H}{l} + \frac{H^2}{l\rho} + \frac{H^2}{l^2} \right). \quad (10)$$

The total current is calculated by integration of current density from Eq. (1) over a hyperboloid surface

$$J_{total} \approx \int j ds. \quad (11)$$

We note that the exchange and correlation effect is ignored in the basic equation (1). Thus the Fowler-Nordheim theory is suitable only for approximate calculations. Nevertheless this theory is widely used for analysis of field emission current from elongated nanostructures. After substitution of field distribution over the sphere surface and an infinitesimal surface element we have

$$\int j ds = \frac{2\pi C_1 V^2}{\phi \sqrt{1 - \tau_0^2} \operatorname{arctanh}^2 \tau_0} \int_1^\infty \frac{\exp\left(-C_2 V^{-1} \phi^{3/2} a \sqrt{(1 - \tau_0^2)(\sigma^2 - \tau_0^2)} \operatorname{arctanh} \tau_0\right)}{\sqrt{\sigma^2 - \tau_0^2}} d\sigma. \quad (12)$$

If $\rho \ll l$ then $\tau_0 \approx 1$ and $\sqrt{\sigma^2 - \tau_0^2} \approx \sqrt{\sigma^2 - 1} \approx \sqrt{2(\sigma - 1)}$. This approximation allows us to reduce our integral to another one $\int_1^\infty \frac{\exp(-a\sqrt{x-1})}{\sqrt{x-1}} dx = \frac{2}{a}$.

Thus the total field emission current is

$$J_{total} \approx \frac{2\pi C_1 V^3 \sqrt{1 + \lambda}}{C_2 \phi^{5/2} \rho \operatorname{arctanh}^3 \sqrt{1/(1 + \lambda)}}, \quad (13)$$

where the total current, J_{total} is measured in A; the radius of curvature, ρ is measured in cm.

3.3.2 Hemisphere on a plane

The metallic sphere in a uniform electric field E_0 (Fig. 5(b)) was considered in many papers (for example Refs. (Forbes et al., 2003; Wang et al., 2004; Pogorelov et al., 2009)). We can replace the sphere by point electric dipole. If the electric dipole moment is p_0 then the dipole potential is

$$\varphi_{dip} = -\frac{p_0}{4\pi\epsilon_0} \frac{z}{(z^2 + r^2)^{3/2}}. \quad (14)$$

Equation of circle is $\varphi_{dip} + zE_0 = 0$. From this equation we can find the relation between the electric dipole moment and the sphere radius: $p_0 = 4\pi\epsilon_0 E_0 \rho^3$. The electric field on the top of hemisphere reaches $E_{top} = p_0 / 2\pi\epsilon_0 \rho^3 + E_0 = 3E_0$. The field enhancement factor is $\beta = E_{top} / E_0 = 3$. The field distribution over the sphere surface have the form $E = 3E_0 \cos \theta$, where θ is polar angle.

Pogorelov et al. (Pogorelov et al., 2009) have shown that the total current emitted from the hemisphere surface is

$$J_{total} = \frac{2\pi\rho^2 C_1 \phi^{7/2} C_2^3}{3E_0} \left[\frac{E_1(C_3)}{6} + \left(\frac{1}{3C_3^3} - \frac{1}{6C_3^2} + \frac{1}{6C_3} \right) \exp(-C_3) \right], \tag{15}$$

where $C_3 = C_2 \phi^{3/2} / 3E_0$ and $E_1(x) \equiv \int \exp(-xt) / t dt$ is the exponential integral.

Due to small β for the hemisphere we need to use very strong electrical field to produce slightly visible current in experiment.

3.3.3 Floating sphere at emitter-plane potential

The “floating sphere at emitter-plane potential” model has no “body” of the field emitter and possesses only its “head”. This model gives too high estimation of electric field on the apex of nanotube but plausibly reproduce tendencies of change of the field enhancement factor. Approximate analytical solution for the “floating sphere at emitter-plane potential” model is well known (for example Refs. (Forbes et al., 2003; Wang et al., 2004)). To solve this problem the method of images (Jackson, 1999) is usually used.

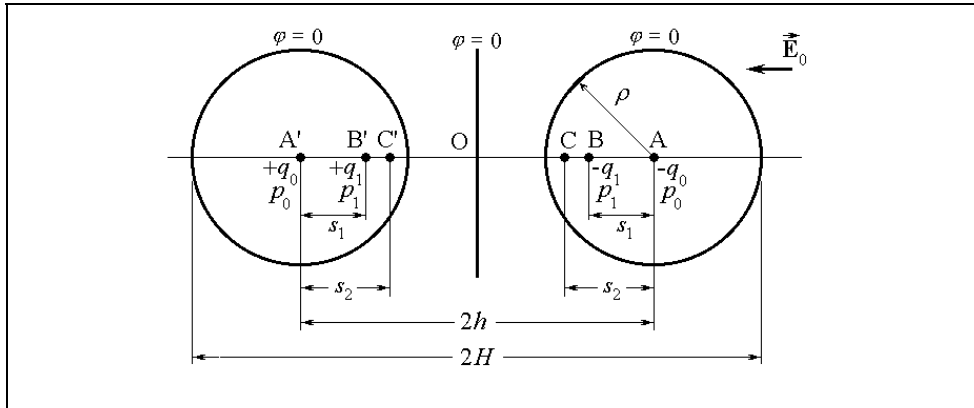


Fig. 7. Two conducting spheres of radius ρ at cathode potential in uniform electric E_0 .

The charge $-q_0 = -4\pi\epsilon_0 h E_0 \rho$ and the electric dipole $p_0 = 4\pi\epsilon_0 E_0 \rho^3$ placed at point A (Fig. 7) create a sphere of radius ρ and potential $\varphi = 0$ in uniform external electric field. The charge q_0 and dipole p_0 cause a potential variation across the emitter plane. To correct this we have to place an image-charge q_0 and image-dipole p_0 at point A' behind the emitter plane. The image-charge and image-dipole will distort the surface of sphere. To restore the shape we should place additional charge $-q_1 = -q_0 \rho / 2h$ and dipole $p_1 = p_0 \rho^3 / 8h^3$ at point B on the distance $s_1 = \rho^2 / 2h$ from the center of sphere (see Fig. 7).

Next we have to put q_1 and p_1 at point B', after to put $-q_2$ and p_2 at C and so on. Neglecting terms of higher smallness in this series of approximation we find the electric field on the top of floating sphere

$$E_{top} = \frac{1}{4\pi\epsilon_0} \frac{q_0}{\rho^2} + \frac{2p_0}{4\pi\epsilon_0} \frac{1}{\rho^3} + \frac{1}{4\pi\epsilon_0} \frac{q_1}{(s_1 + \rho)^2} + E_0 \approx E_0 \left(\frac{h}{\rho} + 3.5 \right). \tag{16}$$

Thus the field enhancement factor is

$$\beta = \frac{1}{\eta} + 3.5 = \frac{H}{\rho} + 2.5. \quad (17)$$

We can provide more accurate calculations. Recurring formulas for the distance s_{i+1} , the charge q_{i+1} , and the dipole moment p_{i+1} through s_i , q_i , and p_i are the following

$s_{i+1} = \frac{\rho^2}{2h - s_i}$, $p_{i+1} = p_i \frac{\rho^3}{(2h - s_i)^3}$, and $q_{i+1} = q_i \frac{\rho}{2h - s_i} - p_i \frac{\rho}{(2h - s_i)^2}$, where the initial distance is zero: $s_0 = 0$.

Series expansion of the field enhancement factor is

$$\beta = \eta^{-1} + \frac{7}{2} - \frac{1}{2}\eta + \frac{1}{8}\eta^2 + \frac{7}{16}\eta^3 - \frac{25}{32}\eta^4 + \frac{25}{32}\eta^5 + O(\eta^6). \quad (18)$$

As the next step of approaching to CNT film, consider an assembly of floating spheres and a screening of the individual emitter by neighbors. The view from above of the sphere surrounded by another one is shown in Fig. 8. Large red circles in this picture are the floating spheres. Small black circles mark places where charges are located. Numbers "0" show initial charges in the center of balls. Numbers "1" specify image charges induced only by nearest neighbors. Numbers "2" concern to secondary image charges.

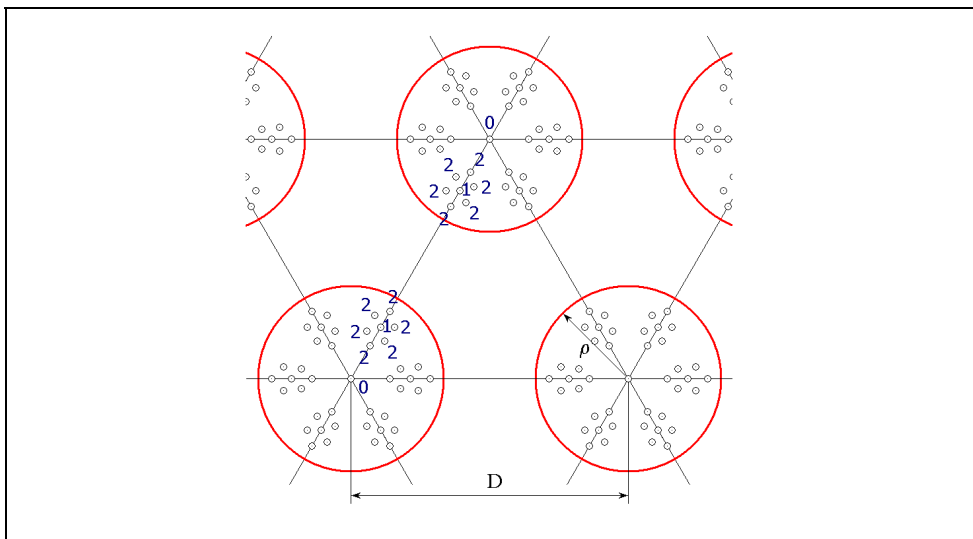


Fig. 8. Honeycomb structure, distance between spheres is D , sphere radius is ρ .

If the distance between spheres, D is large enough ($D \gg \rho$) then all image charges collect on small area around the center of sphere. In that case we can combine all charges inside the ball into its center. Also we will neglect influence of image dipoles.

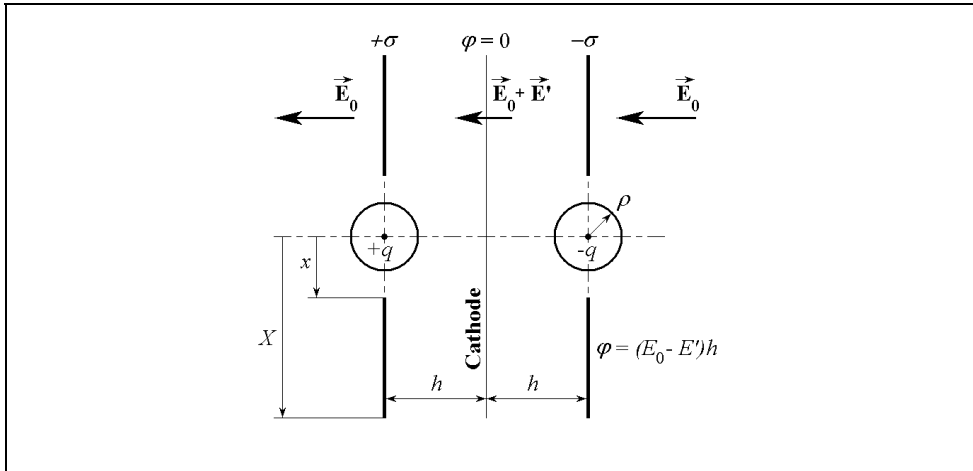


Fig. 9. Modeling of screening effect for floating spheres.

The set of floating spheres produces an idealized surface charge density $\sigma = 2q/\sqrt{3}D^2$. Positively and negatively charged surfaces form the parallel plate capacitor (Fig. 9). The electric field between two large parallel plates is given by $E' = \sigma/\epsilon_0$.

From the equation $h\left(E_0 - \frac{2}{\sqrt{3}\epsilon_0} \frac{q}{D^2}\right) = \frac{1}{4\pi\epsilon_0} \frac{q}{\rho}$ we can find the total charge in the center of each sphere $q = \epsilon_0 h E_0 \left(\frac{1}{4\pi\rho} + \frac{2h}{\sqrt{3}D^2}\right)^{-1}$.

Thus we can find the maximal field on the surface of floating sphere

$$E_{top} = \frac{hE_0}{\rho} \left(\frac{\sqrt{3}D^2}{\sqrt{3}D^2 + 8\pi\rho h}\right) + E_0 \tag{19}$$

and the field enhancement factor

$$\beta = \frac{\sqrt{3}}{\sqrt{3}\eta + 8\pi\delta^2} + 1. \tag{20}$$

More accurate approximation

$$\varphi_{\sigma^+} = 2\pi \int_x^x \frac{\sigma}{4\pi\epsilon_0} \frac{r}{\sqrt{(2h + \rho)^2 + r^2}} dr, \quad \varphi_{\sigma^-} = -2\pi \int_x^x \frac{\sigma}{4\pi\epsilon_0} \frac{r}{\sqrt{\rho^2 + r^2}} dr, \quad x = \sqrt{\frac{\sqrt{3}}{2\pi}} D. \tag{21}$$

$$\varphi_{p^*} = \lim_{x \rightarrow \infty} (\varphi_{\sigma^+} + \varphi_{\sigma^-}) + \frac{1}{4\pi\epsilon_0} \left(\frac{q'}{2h + \rho} - \frac{q'}{\rho}\right). \tag{22}$$

Solving equation $\varphi_{p^*} = E_0 h$ we find

$$\beta = \frac{6(1+\eta)^2}{4\sqrt{6\pi}\delta(1+\eta)\left(\sqrt{2\pi\delta^2(2+\eta)^2 + \sqrt{3}\eta^2} - \eta\sqrt{2\pi\delta^2 + \sqrt{3}}\right) + 3\eta(2+\eta)}. \quad (23)$$

Eq. (23) is transformed to Eq. (20) after neglect in values of higher order of smallness. On the one hand the field enhancement factor and the current density on nanotube apex reach its maximum if the distance between emitters is very large. On the other hand in this case the current density on the anode will be very small. Clearly we can find optimum distance between emitters. As an approximation, assume that the emitting surface of each sphere equals $\pi\rho^2$ and that the electric field is a constant on this surface. The anode current density takes the form

$$\mathbf{j}_{\text{anode}} \approx \frac{2\pi}{\sqrt{3}}\delta^2 \frac{C_1(\beta\mathbf{E}_0)^2}{\phi} \exp\left(-\frac{C_2\phi^{3/2}}{\beta\mathbf{E}_0}\right). \quad (24)$$

If $h \gg \rho$ and $D \gg \rho$ then $\beta \approx \sqrt{3} / (\sqrt{3}\eta + 8\pi\delta^2)$. Let's use this relation for the simplicity.

Solving the equation

$$\frac{\partial \mathbf{j}_{\text{anode}}}{\partial \delta} = 0 = 24\pi\mathbf{E}_0\delta^2 - 3\sqrt{3}\mathbf{E}_0\eta + 24\pi\phi^{3/2}\delta^2 C_2\eta + 64\sqrt{3}\pi^2 C_2\phi^{3/2}\delta^4 \quad (25)$$

we find the optimal dimensionless distance between emitters in honeycomb structure

$$\delta_{\text{opt}} = \left(\frac{3\mathbf{E}_0\eta}{4\pi\left(\sqrt{3}\mathbf{E}_0 + \sqrt{3}C_2\phi^{3/2}\eta + \sqrt{3\mathbf{E}_0^2 + 18C_2\mathbf{E}_0\phi^{3/2}\eta + 3C_2^2\phi^3\eta^2}\right)} \right)^{1/2}. \quad (26)$$

After neglect terms of higher smallness we can write the simplification

$$\delta_{\text{opt}} \approx \sqrt{\frac{\sqrt{3}\mathbf{E}_0\eta}{4\pi(\mathbf{E}_0 + 2C_2\phi^{3/2}\eta)}}. \quad (27)$$

Fig. 10 illustrates the dependence of anode current density from geometrical parameters of emitter. We have assumed that the work function is $\phi = 4.8$ eV, the external field is $E_0 = 60000$ Vcm⁻¹, the dimensionless height is $\eta = 0.001$ (for Fig. 10a), and the dimensionless distance between emitters is $\delta = 0.002$ (for Fig. 10b).

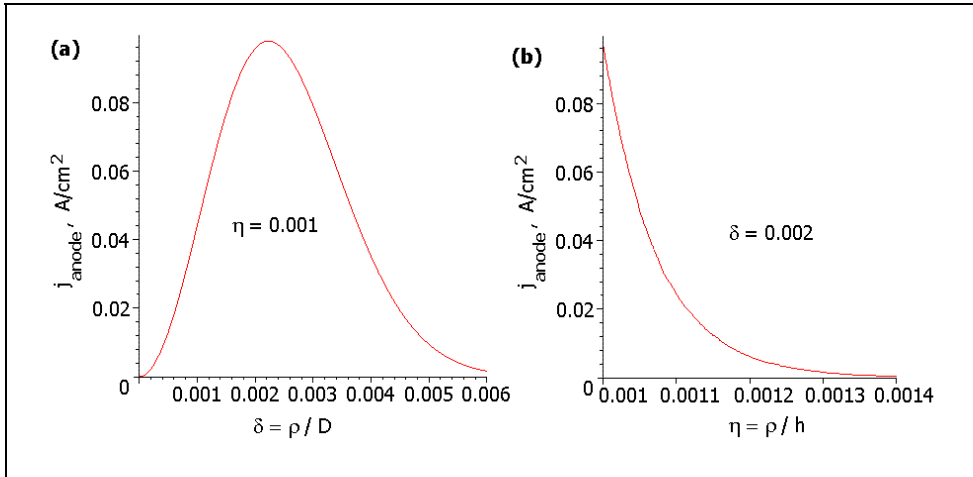


Fig. 10. Anode current density versus dimensionless sizes: (a) optimal distance between emitters if the height is fixed; (b) influence of emitter height on anode current if the density of emitting centers is constant.

Let's consider influence of the limited anode-cathode distance (Fig. 11.) on the field enhancement factor.

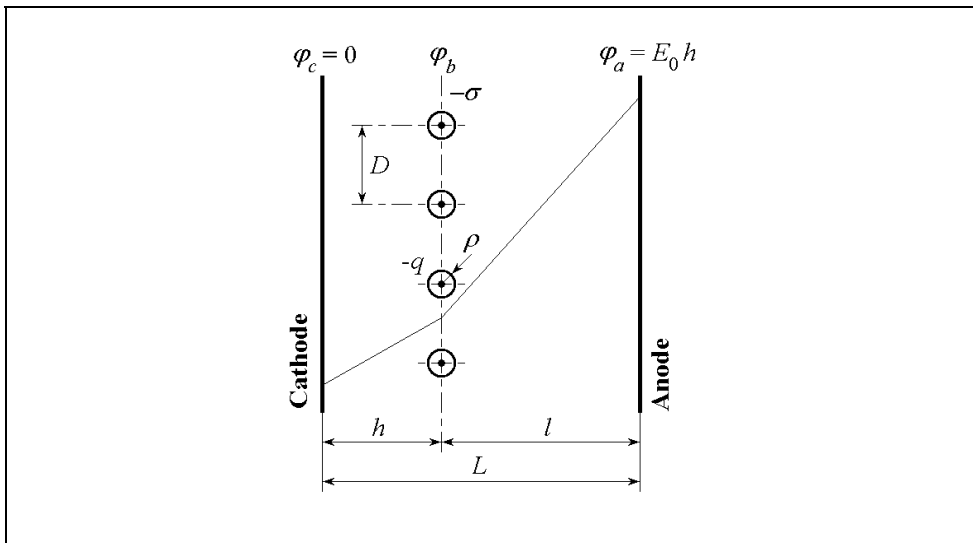


Fig. 11. Geometrical model for the limited distance, L between cathode and anode.

The cathode has zero potential $\varphi_c = 0$; $\varphi_a = E_0 L$ is the anode potential.

As before, assume that average charge per each conductive ball, q is concentrated at its center. Equation for average potential φ_b on plane with grounded conductive balls is

$$-\frac{\varepsilon_0}{h} \varphi_c + \left(\frac{\varepsilon_0}{h} + \frac{\varepsilon_0}{l} \right) \varphi_b - \frac{\varepsilon_0}{l} \varphi_a = -\sigma. \quad (28)$$

Solving the equation $-\frac{2hl}{\sqrt{3}L\varepsilon_0D^2}q + E_0h = \frac{1}{4\pi\varepsilon_0\rho}q$, we find the charge in the center of ball

$$q = \frac{4\sqrt{3}\pi\varepsilon_0E_0h\rho D^2L}{\sqrt{3}D^2L + 8\pi h\rho L - 8\pi h^2\rho}. \quad (29)$$

Thus the maximal field on the surface of floating sphere is

$$E_{top} = \frac{E_0h}{\rho} \left[1 + \frac{8\pi}{\sqrt{3}} \frac{h\rho}{D^2} \left(1 - \frac{h}{L} \right) \right]^{-1}. \quad (30)$$

The field enhancement factor is

$$\beta = \left[\frac{\rho}{h} + \frac{8\pi}{\sqrt{3}} \left(\frac{\rho}{D} \right)^2 \left(1 - \frac{h}{L} \right) \right]^{-1} = \left[\eta + \frac{8\pi}{\sqrt{3}} \delta^2 \left(1 - \frac{\lambda}{\eta} \right) \right]^{-1}. \quad (31)$$

Let us note here that the model of floating sphere and the method of images allow considering field emission not only on flat anode but also on spherical anode.

3.3.4 Hemi-ellipsoid on a plane

Consider a prolate metallic spheroid in a uniform electric field. We can replace the spheroid by a linearly charged thread as we show in our recent paper (Pogorelov et al., 2009). The thread is a green line in Fig. 12 and the linear charge distribution is represented by a red line. The length of a thread is $2h$. The electrostatic potential produced by the charged thread is

$$\varphi(z, r) = - \int_{-h}^h \frac{1}{4\pi\varepsilon_0} \frac{\tau z' dz'}{\sqrt{(z'-z)^2 + r^2}}, \quad (32)$$

where $(r; z)$ denotes the in-plane radial and z coordinates, τz is the linear charge density at point $(0; z)$, h is half of the thread length. The solution is independent of the azimuthal angle. We assume the coefficient of linear charge density, τ to be positive.

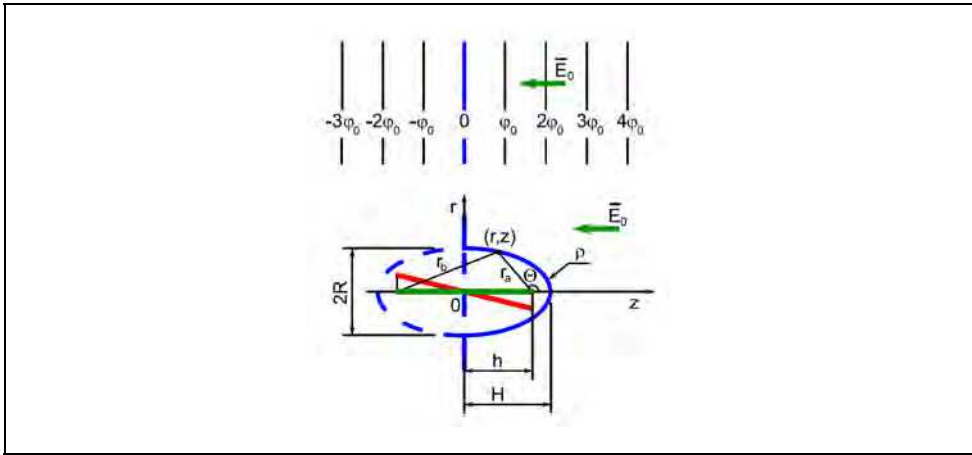


Fig. 12. Linearly charged thread in a uniform electric field along z.

The shape of metallic spheroid is given by the solution to the equation.

$$\varphi(z, r) + E_0 z = 0 . \tag{33}$$

Using coordinates on the spheroid surface $r_a = \sqrt{(z-h)^2 + r^2}$ and $r_b = \sqrt{(z+h)^2 + r^2}$ and a dimensionless parameter, the eccentricity $\xi = \frac{2h}{r_a + r_b}$, ($0 < \xi < 1$), we can rewrite Eq. (33) in the form

$$\frac{4h}{r_a + r_b} - \ln\left(\frac{r_a + r_b + 2h}{r_a + r_b - 2h}\right) = -C , \text{ where } C = 4\pi\epsilon_0 \frac{E_0}{\tau} = \ln\left(\frac{1+\xi}{1-\xi}\right) - 2\xi . \tag{34}$$

The zero equipotential which represents the metallic hemi-ellipsoidal cathode on a plate is shown in Fig. 12 by solid blue line. Points (0, -h) and (0, h) are the foci of the ellipse, r_a and r_b are distances between (r; z) and the two foci.

If ξ is close to 1, the ellipse becomes elongated. If $\xi \rightarrow 0$ the ellipse turns into a circle. Therefore, by changing the coefficient of linear charge density, τ we may modify the shape of the ellipse.

We can also adjust other geometrical parameters of the ellipse: the length of semi-major axis or height H ; the length of semi-minor axis or base radius, R at $z = 0$; and radius of curvature, ρ at point (0, H) (see Fig. 13).

$$H = \frac{h}{\xi} = \frac{r_a + r_b}{2} , R = \frac{h\sqrt{1-\xi^2}}{\xi} , \rho = \frac{R^2}{H} . \tag{35}$$

We can calculate components of the electric field on the surface of the metallic spheroid:

$$E_z = -\frac{E_0}{C} \frac{h(r_b - r_a)^2}{r_a r_b (r_b + r_a)}, E_r = -\frac{E_0}{C} \frac{h(r_b - r_a) \sqrt{4h^2 - (r_b - r_a)^2}}{r_a r_b \sqrt{(r_b + r_a)^2 - 4h^2}}. \tag{36}$$

Thus the modulus of the electric field is

$$E = \sqrt{E_z^2 + E_r^2} = \frac{E_0}{C} \frac{4h^2(r_b - r_a)}{(r_b + r_a) \sqrt{r_a r_b [(r_b + r_a)^2 - 4h^2]}}. \tag{37}$$

Eqs. (36), (37) allow determining the electric field strength on the surface of the half ellipsoid at an arbitrary point. The field enhancement factor at the apex of the ellipsoid is as follows:

$$\beta = \frac{2\xi^3}{(1 - \xi^2)C} = \frac{2\xi^3}{(1 - \xi^2) \left(\ln \frac{1 + \xi}{1 - \xi} - 2\xi \right)}. \tag{38}$$

Analytical expressions for field strength on the z-axis and for field enhancement factor on the tip of the half ellipsoid obtained previously (Forbes et al., 2003; Kosmahl, 1991; Latham, 1981; Latham, 1995) are in agreement with our result. Here, by taking gradient of Eq. (33) we can obtain the field strength at any point we desire. In the limit $\xi \rightarrow 0$ we have a metallic half sphere and the field enhancement factor $\beta = 3$. If $\xi \rightarrow 1$ then for the elongated metallic needle, we have

$$\beta \approx 2 \frac{H}{\rho} \frac{1}{\ln(4H / \rho) - 2}. \tag{39}$$

Ponderomotive forces. Let us estimate the electric force acting on the surface of ellipsoid. We can calculate the force acting on the spheroid surface between circles $r_a = A$ and $r_a = B$ (see Fig. 13).

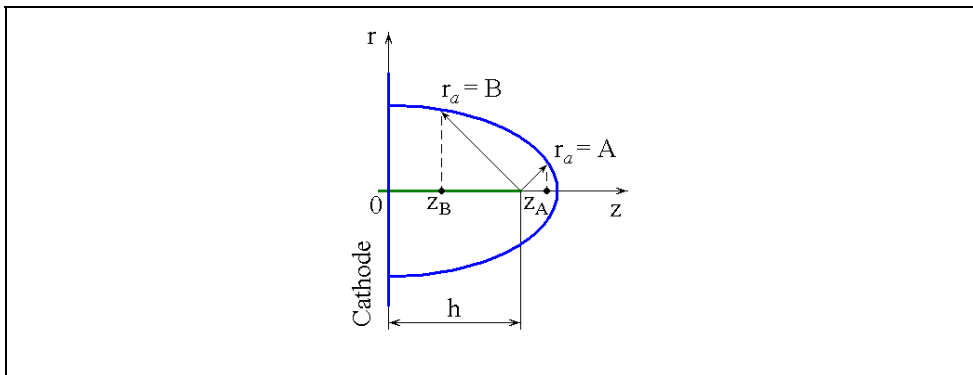


Fig. 13. Geometry for the calculation of ponderomotive force acting on the belt between $r_a = A$ and $r_a = B$.

Thank You for previewing this eBook

You can read the full version of this eBook in different formats:

- HTML (Free /Available to everyone)
- PDF / TXT (Available to V.I.P. members. Free Standard members can access up to 5 PDF/TXT eBooks per month each month)
- Epub & Mobipocket (Exclusive to V.I.P. members)

To download this full book, simply select the format you desire below

